Article

Not peer-reviewed version

Testing Cosmic Acceleration from the Late-Time Universe

Jose Agustin Lozano Torres *

Posted Date: 23 August 2023

doi: 10.20944/preprints202308.1594.v1

Keywords: dark energy; cosmological parameters; numerical methods

Article

Testing Cosmic Acceleration from the Late-Time Universe

Jose Agustin Lozano Torres

Instituto de Física, Universidad Nacional Autónoma de México, Ciudad de México, C.P. 04510, México; jalozanotorres@gmail.com

Abstract: We measure the accelerated cosmic expansion rate of the late-time Universe and derive constraints on cosmological parameters from the final baryon acoustic oscillation (BAO) uncorrelated measurements of different surveys after two decades of dedicated spectroscopic observation combined with the Pantheon sample of Type Ia supernovae, the Hubble diagram of gamma-ray bursts & quasars data, the Cosmic Chronometers data, and the recent Hubble constant value measurement from the Hubble Space Telescope and the SH0ES Team as an additional prior. In Λ cold dark matter (ΛCDM) scenario, the model fit yields $\Omega_m = 0.313 \pm 0.034$ and $\Omega_\Lambda = 0.672 \pm 0.025$. Combining BAO with CC+Pantheon+QSR+GRB data sets we get $H_0 = 69.21 \pm 1.22$ km s^{-1} Mpc^{-1}, $r_d = 133.46 \pm 2.49$ Mpc. For the a flat wCDM model, we get $w = -1.111 \pm 0.030$. For a dynamical evolution of dark energy in a flat w_0w_aCDM cosmology, we get $w_a = -0.292 \pm 0.167$. We apply the Akaike information criteria probe to compare the three models, and see that all models are favored and cannot be discarded from the current data.

Keywords: dark energy; cosmological parameters; numerical methods

1. Introduction

The values of cosmological parameters of the standard model of cosmology have been estimated and highly constrained through various observational experiments [1,2] with unprecedented accuracy. The observational measurements results from Planck 2018 define the "cornerstone" of constraints for the cosmological key parameters, such as the Hubble constant H_0. Although the Hubble constant cannot be measured directly by the cosmic microwave background (CMB) Planck satellite, it is measured once the other cosmological parameters are known through a global analysis fitting in the ΛCDM scenario. In the LCDM scenario, [1] estimated the value of the Hubble constant at $H_0 = 67.4 \pm 0.5$ km s^{-1} Mpc^{-1} whose uncertainty is below 1 km s^{-1} Mpc^{-1}. However, measurements in the local neighborhood at low redshifts of the Hubble constant [3–7] have caused tension and, ironically, a window of opportunity to test alternative models beyond the ΛCDM model. In particular, SH0ES project [4] developed a distance ladder method from standard candles known as cepheids stars to estimate H_0. Currently, they have been improving the value of H_0 with more precision and obtain the updated results as $H_0 = 73.04 \pm 1.04$ km s^{-1} Mpc^{-1} [7]. Despite the success of the LCDM model, the current measurements of late-time accelerated cosmic expansion [7] and early-time measurements [1] countered each other, causing a crisis in cosmology known as Hubble tension whose discrepancy between them is situated in the range of 4σ–5.7σ. Such discrepancy implicates that either early-and-late time measurements have systematics and calibration issues or the standard cosmological model fails to describe the universe. Furthermore, this tension may provide a hint of new physics beyond the standard model. Following this motivation, a wide range of alternative cosmological models have been proposed to alleviate inconsistencies between data surveys [8–20]. In the opposite case, many studies have been made to provide estimates of the Hubble constant on other observations, such as quasar lensing [21,22], gravitational-wave events [23–25], fast radio bursts (FRBs) [26,27], Megamaser [28–30], red giant branch tip method (TRGS) [31–33], BAOs [34], etc [35]. For example, the H0LiCOW research group [36] exhibits another method to estimate H_0 by the time delay from gravitational lensing effects. In a flat ΛCDM scenario, they estimate a value of $H_0 = 73.3^{+1.7}_{-1.8}$ km s^{-1} Mpc^{-1} [37]. The Advanced

Preprints (www.preprints.org) | NOT PEER-REVIEWED | Posted: 23 August 2023 doi:10.20944/preprints202308.1594.v1

LIGO and Virgo research teams detected a gravitational-wave event GW170817 coming from the merger of a binary neutron-star system. They determine the Hubble constant to be $H_0 = 70^{+12.0}_{-8.0}$ km s^{-1} Mpc^{-1}[38]. These observations do present an advantage: they are independent from the CMB surveys and distance ladder measurements, allowing to offer an answer to the different observed H_0 tensions. As for baryons acoustic oscillations (BAOs), which are a matter of interest in our study, they are sound waves traveling in the primordial baryon-photon fluid, frozen at the recombination epoch. These oscillations are found in the clustering of large-scale structures by different independent observational surveys. Such BAOs surveys give measurement results in terms of $D_A(z)/r_d$, $D_V(z)/r_d$, and $H(z)\cdot r_d$, where r_d is the comoving size of sound horizon at drag epoch. As it is well-known, at recombination era, the photons decouple from the baryons at first, at $z_* \approx 1090$, giving rise to the CMB. The baryons do not feel the drag of photons until $z_d \approx 1059$, which sets the standard ruler for the BAOs. The Hubble constant H_0 and the sound horizon r_d are strongly related, forming the so called $H_0 - r_d$ plane, linking the early-and-late time universe. In general, r_d relies on the physical conditions of the early universe, which can be constrained by precise CMB observations. In most all of BAO measurements, the constraint on the Hubble constant by using BAO data is not entirely independent on the CMB data [39]. Instead of early time physical calibration of r_d, an alternative method is to combine BAO measurements with other low-redshift observations.

In this study, we select the final BAO measurements results from different observational experiments [40–50] covering 17 BAO data points and test whether these BAO points could be correlated or not. According to [51], despite the existence of large galaxy survey data sets, it is recommendable to use a small sample to minimize correlations among the selected data points, thus reducing the errors. One way is to test the concordance of the set against the incorporation of random correlations and perform the analysis on the cosmological parameters. Furthermore, in our analysis we consider the ΛCDM, wCDM, and w_0w_aCDM cosmological models. Combining the final BAO measurements with the Pantheon type Ia supernovae, the cosmic chronometers data set, the Hubble diagram of gamma-ray bursts and quasars, and the latest measurement of the Hubble constant [7] as an additional prior, we estimate the sound horizon r_d and the Hubble constant H_0. The structure of the paper is the following: In section 2 we present the cosmological models under study. The data sets and methodology are presented in section 3. In Sec. 4 we present our estimated results from the latest low-redshift surveys data sets. In Sec. 5 we discuss our results and present their implications for the cosmological models under study. Finally, we present our conclusions in section 6.

2. Theoretical Background

2.1. Standard Cosmological Model

The Λ cold dark matter (ΛCDM) model takes the simplest form of dark energy as the cosmological constant Λ with equation-of-state $w = -1$, acting as a negative pressure to counteract the effect of gravity. The Friedmann equation for the ΛCDM model expressed in terms of the expansion function is written as

$$E^2(z) = \Omega_r(1+z)^4 + \Omega_m(1+z)^3 + \Omega_\Lambda, \tag{1}$$

where we have set $\Omega_{DE} = \Omega_\Lambda$, with EOS $w = -1$. The Friedmann equation (1) depends on free parameters Ω_r, Ω_m, Ω_Λ. Although the radiation parameter Ω_r is usually not considered for a flat late-universe, we include it for a complete description. The term $E(z)$ is the function rate and is the ratio $H(z)/H_0$, where $H(z) = \dot{a}/a$ is the Hubble parameter at redshift z and H_0 is the Hubble parameter today.

Preprints (www.preprints.org) | NOT PEER-REVIEWED | Posted: 23 August 2023 doi:10.20944/preprints202308.1594.v1

2.2. Flat-Constant-wCDM Model

For this model, we assume that dark energy has a constant equation-of-state w. The Friedmann equation for the wCDM model expressed in terms of the expansion function is written as

$$E^2(z) = \Omega_r(1+z)^4 + \Omega_m(1+z)^3 + \Omega_\Lambda(1+z)^{3(1+w)}, \tag{2}$$

where equation (2) depends on free parameters Ω_r, Ω_m, Ω_Λ and w.

2.3. w0waCDM Model or CPL Parametrization

The parametrization of the dark energy equation-of-state w can be a function of redshift z or the scale factor $a(t)$ of the Friedmann-Lemaitre-Robertson-Walker metric universe, noticing that $1+z = a_0/a(t)$, where a_0 is the present value of the scale factor. Here, we consider a dynamical dark energy equation-of-state w parametrization called Chevallier-Polarski-Linder (CPL) model. This model introduces a parametrization that varies as a function of time. This model is given by [52–54]

$$w(a) = w_0 + (1-a)w_a, \tag{3}$$

or in terms of redshift z,

$$w(z) = w_0 + w_a\frac{z}{1+z}, \tag{4}$$

where w_0 represents the cosmological constant Λ or the current value of the dark energy equation-of-state, that means, $w(z=0) = w_0$ and noticing that $(\frac{\mathrm{d}w(z)}{\mathrm{d}z})_{z=0} = w_a$ one can regard this as a free time parameter. From the CPL parametrization, we can write the Friedmann equation in terms of the expansion function as

$$E^2(z) = \Omega_r(1+z)^4 + \Omega_m(1+z)^3 + \Omega_{DE}(1+z)^{3(1+w_0+w_a)}\exp\Big(-\frac{3w_a z}{1+z}\Big), \tag{5}$$

where equation 5 depend on free parameters Ω_r, Ω_m, Ω_Λ, w_0 and w_a. The measured redshifts and angles on the celestial sphere need to be converted to cosmological distances by adopting a fiducial cosmological model, and the analysis measures the ratio of the observed BAO scale to that predicted in the fiducial cosmological model. The studies of the BAO feature in the transverse direction provide a measurement of $D_H(z)/r_d = c/H(z)r_d$, with the comoving angular diameter distance in a flat-space,

$$D_M = \frac{c}{H_0}\int_0^z \frac{\mathrm{d}z'}{E(z')}. \tag{6}$$

Furthermore, BAO data are also expressed in cosmological observables such as angular diameter distance $D_A = D_M/(1+z)$ and the $D_V(z)/r_d$, which encodes the BAO peak coordinates information,

$$D_V(z) = [zD_H(z)D_M^2(z)]^{1/3}, \tag{7}$$

where r_d is the cosmic sound horizon at the drag epoch measured by [1] in $r_d = 147.1$ Mpc.

3. Data and Methodology

For the exploration of the late-time cosmic expansion of the Universe, we use a main collection of points of the latest BAO measurements from different observational experiments. The data points come from the Sloan Digital Sky Survey (SDSS) [42,49], BOSS [43] , eBOSS [45–48]. In addition, we also include data measurements from the WiggleZ Dark Energy Survey [41], the Dark Energy Survey (DES) [50], the Dark Energy Camera Legacy Survey (DECaLS) [44], and 6dFGS BAO [40]. The BAO data points are listed in Table 1 with their corresponding redshifts z_{eff}, observables, measurements,

Preprints (www.preprints.org) | NOT PEER-REVIEWED | Posted: 23 August 2023 doi:10.20944/preprints202308.1594.v1

and errors. Although these observational surveys are independent from each other, it is possible that these measurements could be correlated between them.

Table 1. Sample of BAO uncorrelated data points on which we perform our analysis.

z_{eff}	Observable	Measurement	Error	Year	Data Set Survey	Reference
0.106	r_d/D_V	0.3366	0.015	2011	6dFGS BAO	[40]
0.11	D_A/r_d	2.607	0.138	2021	SDSS Blue Galaxies sample	[49]
0.15	$D_V(r_d/r_{d,fid})$	664	25	2015	SDSS Main Galaxy Sample	[42]
0.38	$D_V(r_d/r_{d,fid})$	1477	16	2017	BOSS DR12 Galaxies	[43]
0.44	$D_V(r_d/r_{d,fid})$	1716	83	2014	WiggleZ Dark Energy Survey	[41]
0.51	$D_V(r_d/r_{d,fid})$	1877	19	2017	BOSS DR12 Galaxies	[43]
0.6	$D_V(r_d/r_{d,fid})$	2221	101	2014	WiggleZ Dark Energy Survey	[41]
0.61	$D_V(r_d/r_{d,fid})$	2140	22	2017	BOSS DR12 Galaxies	[43]
0.697	$D_A(r_d/r_{d,fid})$	1529	73	2020	DECaLS DR8 Footprint LRG Sample	[44]
0.698	D_H/rd	19.77	0.47	2020	eBOSS DR16 LRG Sample	[45]
0.73	$D_V(r_d/r_{d,fid})$	2516	86	2014	WiggleZ Dark Energy Survey	[41]
0.835	D_A/r_d	18.92	0.51	2022	DES Year 3	[50]
0.845	$D_V(r_d/r_{d,fid})$	18.32	0.58	2020	eBOSS DR16 LRG Sample	[46]
0.874	$D_A(r_d/r_{d,fid})$	1674	102	2020	DECaLS DR8 Footprint LRG Sample	[44]
1.48	D_H/r_d	13.11	0.52	2020	eBOSS DR16 Quasar Sample	[47]
2.33	D_A/r_d	37.5	1.1	2020	eBOSS DR16 Lyα-Quasar	[48]
2.33	D_H/r_d	8.99	0.19	2020	eBOSS DR16 Lyα-Quasar	[48]

Generally, one needs to perform tests simulations in order to evaluate systematic errors and find suitable covariance matrices. Since we use a collection of measurements from different observational surveys, we do not use a precise covariance matrix between them. To overcome this, we follow the covariance analysis given in [51]. The covariance matrix for uncorrelated points is

$$C_{ii} = \sigma_i^2. \tag{8}$$

To simulate the impact of possible correlations among data points, we can introduce non-diagonal elements in an aleatory manner in the covariance matrix but keeping it symmetric. Based on this method, we establish non-negative correlations in up to twelve pairs of chosen data points aleatory which represents around 66.66% of the whole BAO data set given in Table 1. The magnitude of these aleatory chosen covariance matrix element C_{ij} is set to

$$C_{ij} = 0.5\sigma_i\sigma_j, \tag{9}$$

where $\sigma_i\sigma_j$ are the 1σ errors of the data points i, j. We implemented a nested sampling algorithm tailored for high-dimensional parameter space called *Polychord* developed by [55] to perform the calculations. The prior we select is with a uniform distribution given by

$$\Omega_m \in [0.;1], \quad \Omega_{DE} \in [0.;1-\Omega_m], \quad H_0 \in [50;100], r_d \in [100;200], \quad r_d/r_{d,fid} \in [0.9,1.1]. \tag{10}$$

Furthermore, the latest measurement of the Hubble constant estimated by [7] $H_0 = 73.04 \pm 1.04$ km s^{-1} Mpc^{-1} has been integrated into our analysis as an additional prior, which we refer it as R22. The "full-data set" encodes the sum of BAO+CC+Pantheon+QSR+GRB data sets.

4. Results

The results for BAO and the BAO+R22 in the context of random correlations can be observed in Figure 1 and Table 2.

Preprints (www.preprints.org) | NOT PEER-REVIEWED | Posted: 23 August 2023 doi:10.20944/preprints202308.1594.v1

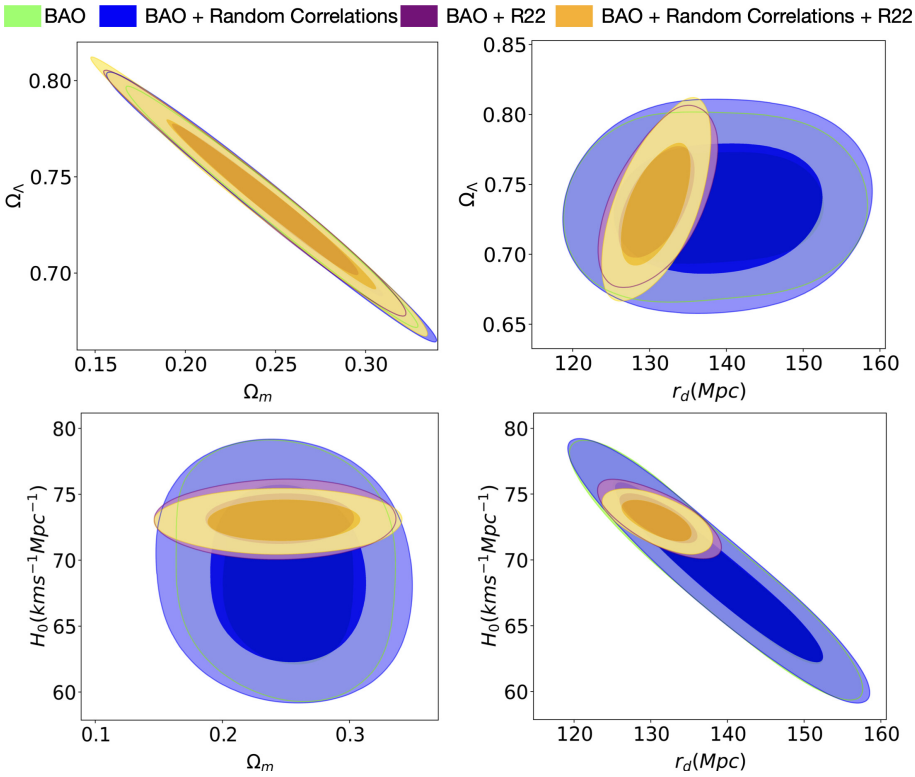

Figure 1. The figure exhibits the posterior distribution for ΛCDM with and without a randomly test covariance matrix with twelve correlated components. The discrepancy between null uncorrelated and twelve correlated components is almost negligible.

Table 2. Variation of some cosmological parameters according to the number of correlated pairs. The values with uncorrelated pairs ($n = 0$) are slightly different when correlated pairs ($n = 12$) are introduced.

n correlated pairs	BAO	BAO + R22
n=0	$\Omega_m = 0.2502 \pm 0.0321$	$\Omega_m = 0.2474 \pm 0.0381$
	$\Omega_\Lambda = 0.7338 \pm 0.0257$	$\Omega_\Lambda = 0.7359 \pm 0.0280$
n=12	$\Omega_m = 0.2587 \pm 0.0178$	$\Omega_m = 0.2571 \pm 0.0290$
	$\Omega_\Lambda = 0.7355 \pm 0.0274$	$\Omega_\Lambda = 0.7371 \pm 0.0239$

By introducing some random correlated pairs change the values of some cosmological parameters. However, the difference between the values from null correlated pairs ($n = 0$) and 66.66% correlated points ($n = 12$) is surprisingly about 1%, allowing us to consider our BAO data set as uncorrelated, which is very low compared to the discrepancy given in [51]. In order to constraint our models, aside the collection of BAO data points listed in Table 1, we use the latest data set of Pantheon sample from the Supernovae Type Ia [56], the Hubble parameter measurements from the Cosmic Chronometers (CC) containing 30 uncorrelated data points [57], the measurements from the Hubble diagram of quasars referred as QSR [58], the measurements from the Hubble diagram of gamma-ray bursts referred as GRB [59], and latest Hubble constant measurement referred as R22 [7] as an additional prior.

4.1. Standard Cosmological Model

We can start evaluating the cosmological models based on the data measurements. For the standard model of cosmology ΛCDM we set H_0, Ω_m, Ω_Λ, r_d, $r_d/r_{d,fid}$ as free parameters. The estimated values for the cosmological parameters in the ΛCDM scenario for different combinations of data sets can be depicted in Figure 2, including the contours of $\Omega_m - H_0$ and $H_0 - r_d$.

Preprints (www.preprints.org) | NOT PEER-REVIEWED | Posted: 23 August 2023 doi:10.20944/preprints202308.1594.v1

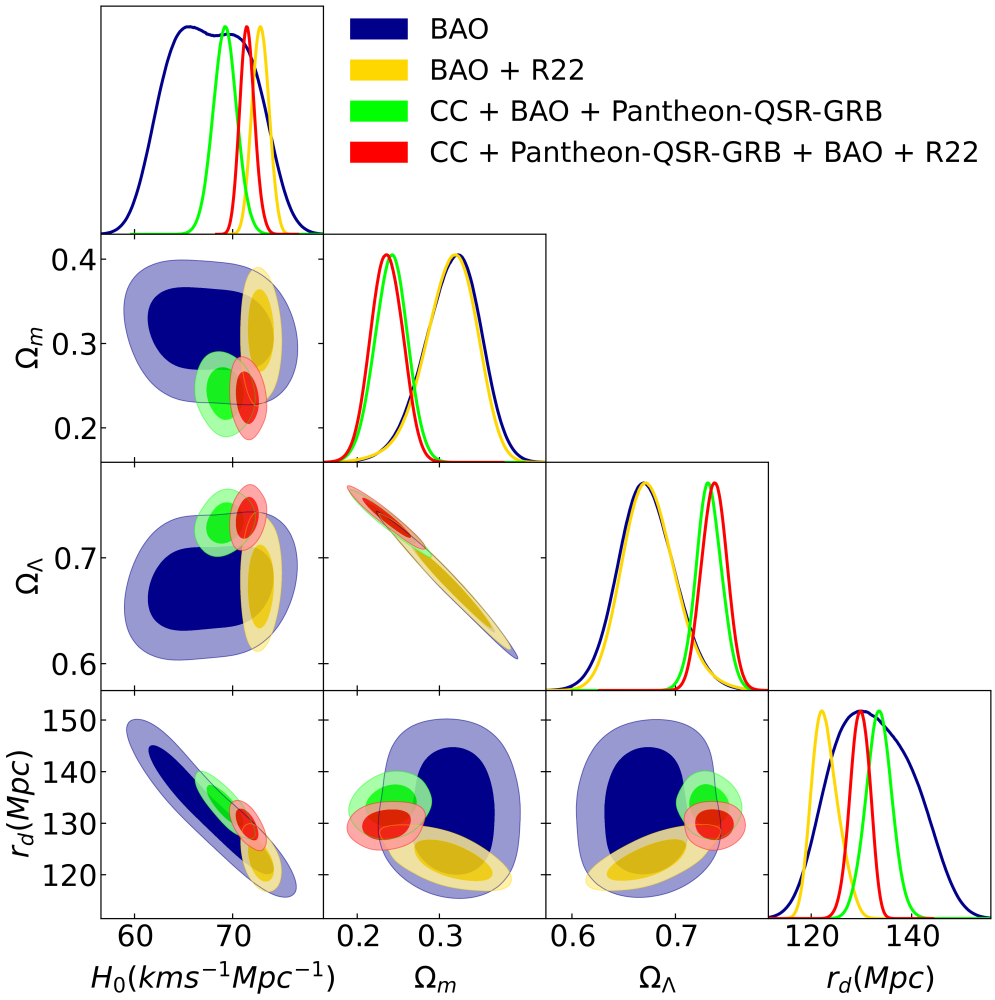

Figure 2. The figure exhibits the posterior distribution for different observational data measurements with the ΛCDM with 1σ and 2σ. The BAO refers to the baryon acoustic oscillations data set from Table 1. The CC data set refers to the cosmic chronometers and Pantheon refers to the Hubble diagram from type Ia supernovae, quasars measurements as QSR, and gamma-ray bursts measurements as GRB. R22 denotes [7] measurement of the Hubble constant as a Gaussian prior.

In Figure 2 is reported the 68% and 95% confidence levels for the posterior distribution. The numerical results of the evaluated cosmological parameters under ΛCDM scenario are listed in Table 3.

Table 3. Constraints at 95% CL on the cosmological parameters for the standard ΛCDM model based on baryon acoustic oscillations (BAO), cosmic chronometers (CC), Pantheon-QSR-GRB, and additional prior R22.

Parameters	BAO	BAO + R22	BAO+CC+Pantheon-QSR-GRB	BAO+R22+CC+Pantheon-QSR-GRB
H_0 [Km s^{-1} Mpc^{-1}]	67.74 ± 4.40	72.85 ± 1.21	69.21 ± 1.22	71.50 ± 1.096
Ω_m	0.3157 ± 0.0341	0.3132 ± 0.0310	0.2411 ± 0.0290	0.2358 ± 0.0281
Ω_Λ	0.6724 ± 0.0254	0.6748 ± 0.0243	0.7325 ± 0.0121	0.7376 ± 0.0125
r_d [Mpc]	132.28 ± 8.66	122.85 ± 2.58	133.46 ± 2.49	129.72 ± 2.90
$r_d/r_{d,fid}$	0.9932 ± 0.0647	0.9218 ± 0.0141	0.9913 ± 0.0179	0.9620 ± 0.0102

When BAO data set alone is regarded, the estimated values of the cosmological parameters are in agreement with [1] measurement results except for r_d. When we incorporate the R22 prior, the fit gives

Preprints (www.preprints.org) | NOT PEER-REVIEWED | Posted: 23 August 2023 doi:10.20944/preprints202308.1594.v1

a estimated value for H_0 away from [1] and closer to the measured one in the SNe sample by [7]. Once again, when we incorporate cosmic chronometers and Pantheon-QSR-GRB samples into BAO, the value of the Hubble constant is closer to that value estimated by [1]. We also observe that the matter-energy density is similar to the value estimated by [1] $\Omega_m = 0.315 \pm 0.007$ when we consider BAO and BAO + R22 and smaller when BAO+CC+Pantheon-QSR-GRB and BAO+CC+Pantheon-QSR-GRB+R22 are taken into account . In the framework of the BAO scale, it is set by the cosmic sound horizon imprinted in the cosmic microwave background at the drag epoch z_d when the see of baryons and photons decouple from each other, according to

$$r_d = \int_{z_d}^{\infty} \frac{c_s(z)}{H(z)} \mathrm{d}z, \tag{11}$$

where the speed of sound is expressed as $c_s = \sqrt{\frac{\delta p_\gamma}{\delta \rho_B + \delta \rho_\gamma}} = \sqrt{\frac{(1/3)\delta \rho_\gamma}{\delta \rho_B + \delta \rho_\gamma}} = \frac{1}{\sqrt{3(1+R)}}$, where $R \equiv \delta \rho_B / \delta \rho_\gamma = \frac{3\rho_B}{4\rho_\gamma}$. The data from [1] gives the redshift at the drag epoch $z_d = 1059.94 \pm 0.30$. For a flat ΛCDM, [1] measurements estimate $r_d = 147.09 \pm 0.26$ Mpc. In our analysis, the posterior distribution of the $r_d - H_0$ contour plane is exposed at the bottom of the first column in Figure 2. [60] finds $r_d = 143.9 \pm 3.1$ Mpc. [63] reports that using Binning and Gaussian methods to combine measurements of 2D BAO and SNe data, the values of the absolute BAO scale range from 141.45 Mpc $\leq r_d \leq$ 159.44 Mpc (Binning) and 143.35 Mpc $\leq r_d \leq$ 161.59 Mpc (Gaussian). The above results demonstrate a clear discrepancy between early-and-late times observational measurements, analogously to the H_0 tension. It should be noticed that our results depend on the range of priors for r_d and H_0, shifting the estimated values in the $r_d - H_0$ contour plane. A noticeable feature is when we don't include the additional prior: the results tend to be in an excellent agreement with [1] results and to the SDSS results, and to [63] when BAO data set alone is considered.

4.2. Models Beyond Standard Model

Aside the standard ΛCDM cosmological model, we test two more cosmological models whose dark energy equation-of-state are non-dynamical, dynamical, and different from $w = -1$: the wCDM model and w_0w_aCDM model. For the wCDM model, we use $w \in [-1.25; -0.75]$, while for the w_0w_aCDM model, we use $w_0 \in [-1.25; -0.75]$ and $w_a \in [1.0; -1.0]$. For the rest of the priors are the same as for ΛCDM.

4.2.1. wCDM Model

This model considers a constant dark energy equation-of-state $w \neq -1$. The results for different combinations of data-sets surveys can be seen in Figure 3 and listed in Table 4. We clearly observe that the dark energy equation-of-state obtained tends to be compatible with the one estimated by [1] which results $w = -1.03 \pm 0.03$ in all data sets combinations.

Preprints (www.preprints.org) | NOT PEER-REVIEWED | Posted: 23 August 2023 doi:10.20944/preprints202308.1594.v1

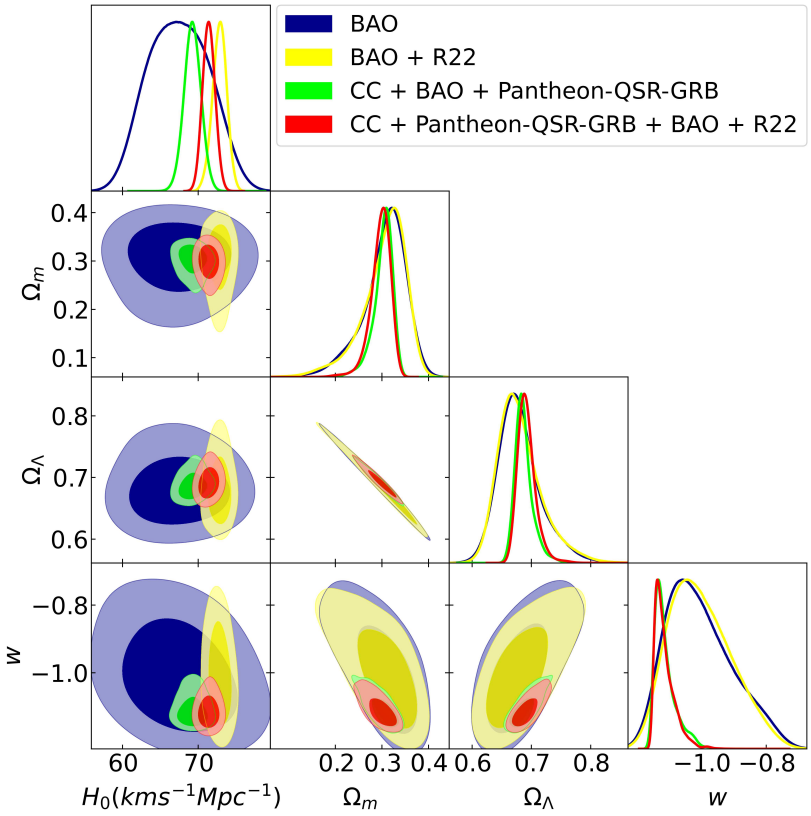

Figure 3. The figure exhibits the posterior distribution for different observational data measurements with the wCDM model with 1σ and 2σ. The BAO refers to the baryon acoustic oscillations dataset from Table 1. The CC data set refers to the cosmic chronometers and Pantheon refers to the Hubble diagram from type Ia supernovae, quasars measurements as QSR, and gamma ray bursts as GRB. R22 denotes [7] measurement of the Hubble constant as a Gaussian prior.

Table 4. Constraints at 95% CL on the cosmological parameters for the wCDM model based on baryon acoustic oscillations (BAO), cosmic chronometers (CC), Pantheon-QSR-GRB, and additional prior R22.

Parameters	BAO	BAO + R22	BAO+CC+Pantheon-QSR-GRB	BAO+R22+CC+Pantheon-QSR-GRB
H_0 [Km s^{-1} Mpc^{-1}]	67.43 ± 4.36	72.82 ± 1.47	69.25 ± 1.06	71.39 ± 1.11
Ω_m	0.3062 ± 0.0433	0.3055 ± 0.0447	0.3026 ± 0.0197	0.2974 ± 0.0187
Ω_Λ	0.6799 ± 0.0325	0.6803 ± 0.0346	0.6871 ± 0.0134	0.6918 ± 0.0147
w	-1.006 ± 0.107	-1.003 ± 0.101	-1.111 ± 0.030	-1.112 ± 0.0286
r_d [Mpc]	133.29 ± 8.30	122.95 ± 2.74	133.08 ± 2.29	129.57 ± 2.64
$r_d/r_{d,fid}$	0.9999 ± 0.0637	0.9231 ± 0.0164	0.9939 ± 0.0151	0.9663 ± 0.0106

The above results imply that we cannot rule out $w = -1$ when we consider all the combinations of different data sets from cosmological objects. In Figure 4 we observe the $r_d - H_0$ in the framework of wCDM model.

Preprints (www.preprints.org) | NOT PEER-REVIEWED | Posted: 23 August 2023 doi:10.20944/preprints202308.1594.v1

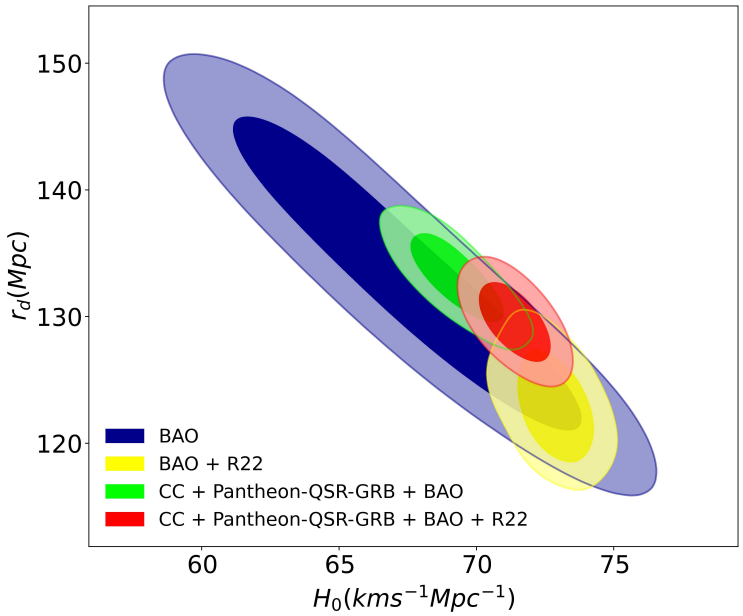

Figure 4. The figure exhibits the posterior distribution for different observational data measurements with the wCDM with 1σ and 2σ in the $r_d - H_0$ contour plane. The BAO refers to the baryon acoustic oscillations data set from Table 1. The CC dataset refers to the cosmic chronometers and Pantheon refers to the Hubble diagram from type Ia supernovae, quasars measurements as QSR, and gamma ray bursts as GRB. R22 denotes [7] measurement of the Hubble constant as a Gaussian prior.

When BAO and BAO+CC+Pantheon-QSR-GRB are considered, our values are in agreement with those values obtained by [61] $r_d = 136.7 \pm 4.1$. Mpc. However, when we incorporate R22 to BAO and BAO+CC+Pantheon-QSR-GRB data sets the sound horizon at drag epoch yields $r_d = 122.95 \pm 2.74$ Mpc and $r_d = 129.57 \pm 2.54$ Mpc, respectively. Our estimated results for r_d are clearly in tension with those estimated by [60] $r_d = 143.9 \pm 3.1$ Mpc, [62] independent of CMB data $r_d = 144 \pm ^{+5.3}_{-5.5}$ Mpc (from $\theta_{BAO} + BBN + HoLiCOW$), and [1].

4.2.2. w0waCDM Model

Our estimated values of the (w_0, w_a) parameters for various data combinations can be seen in Figure 5 and listed in Table 5. It is interesting to observe that our values are in agreement with those obtained by [1] with TT,TE,EE+lowE+lensing with other data-sets: $w_0 = -0.957 \pm 0.080$, $w_a = -0.29^{+0.32}_{-0.26}$ (from *Planck*+SNe+BAO) even though we take different combinations of data-sets. The $r_d - H_0$ plane in the framework of w_0w_aCDM model is presented in Figure 6.

Table 5. Constraints at 95% CL on the cosmological parameters for the w_0w_aCDM model based on baryon acoustic oscillations (BAO), cosmic chronometers (CC), Pantheon-QSR-GRB, and additional prior R22.

Parameters	BAO	BAO + R22	BAO+CC+Pantheon-QSR-GRB	BAO+R22+CC+Pantheon-QSR-GRB
H_0 [Km s^{-1} Mpc^{-1}]	67.88 ± 4.32	72.82 ± 1.20	69.25 ± 1.24	71.43 ± 1.01
Ω_m	0.3074 ± 0.0403	0.3058 ± 0.0408	0.3033 ± 0.0250	0.2989 ± 0.0268
Ω_Λ	0.6802 ± 0.0331	0.6826 ± 0.0315	0.6871 ± 0.0216	0.6914 ± 0.0213
w_0	-0.926 ± 0.126	-0.910 ± 0.123	-0.830 ± 0.0925	-0.828 ± 0.095
w_a	-0.214 ± 0.230	-0.225 ± 0.227	-0.292 ± 0.167	-0.285 ± 0.169
r_d [Mpc]	132.68 ± 8.66	124.09 ± 2.94	132.79 ± 2.21	129.33 ± 2.71
$r_d/r_{d,fid}$	1.000 ± 0.062	0.9334 ± 0.0202	0.9961 ± 0.0162	0.9680 ± 0.0109

Preprints (www.preprints.org) | NOT PEER-REVIEWED | Posted: 23 August 2023 doi:10.20944/preprints202308.1594.v1

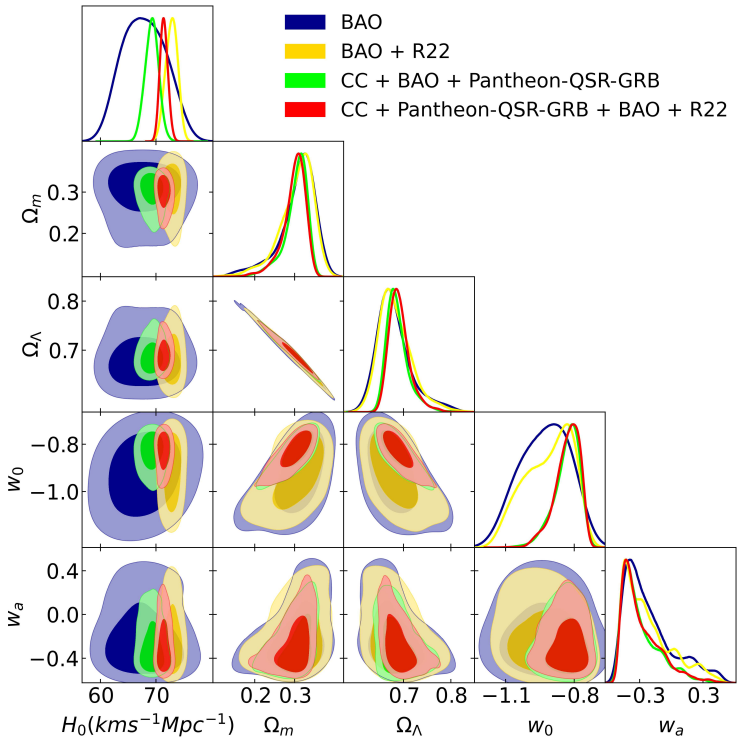

Figure 5. The figure exhibits the posterior distribution for different observational data measurements with the w_0w_aCDM model with 1σ and 2σ. The BAO refers to the baryon acoustic oscillations dataset from Table 1. The CC data set refers to the cosmic chronometers and Pantheon refers to the Hubble diagram from type Ia supernovae, quasars, and gamma ray bursts. R22 denotes [7] measurement of the Hubble constant as a Gaussian prior.

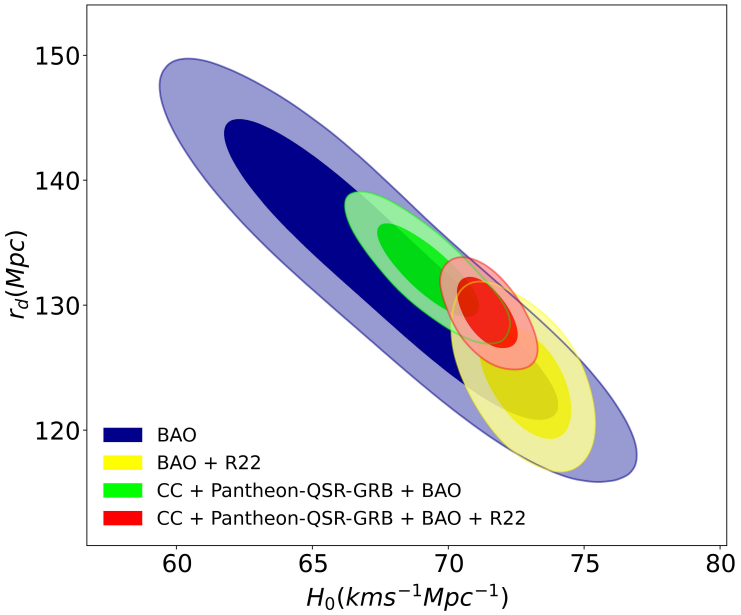

Figure 6. The figure exhibits the posterior distribution for different observational data measurements with the w_0w_aCDM with 1σ and 2σ in the $r_d - H_0$ contour plane. The BAO refers to the baryon acoustic oscillations data-set from Table 1. The CC data set refers to the cosmic chronometers and Pantheon refers to the Hubble diagram from type Ia supernovae, quasars, and gamma ray bursts. R22 denotes [7] measurement of the Hubble constant as a Gaussian prior.

Preprints (www.preprints.org) | NOT PEER-REVIEWED | Posted: 23 August 2023 doi:10.20944/preprints202308.1594.v1

The fit for BAO leads 132.68 ± 8.66 Mpc. Adding CC and Pantheon-QSR-GRB data-sets result 132.79 ± 2.21 Mpc and taking all the data-sets plus R22 prior leads to $r_d = 129.33 \pm 2.71$, creating a tension with [1] results $r_d = 147.09 \pm 0.26$ Mpc and our late-time measurements.

5. Discussion

Our study select 17 data points that represent the latest and final BAO measurements from different observational survey in the last two decades in combination with the cosmic chronometers (30 data points), and the Pantheon type Ia supernova (40 data points), the Hubble diagram for quasars (24 data points), and gamma-ray bursts (162 data points). Although our results based on the latest measurements from different observational tests demonstrate that Hubble tension is still there it has been alleviated: 2.6σ for the H_0. By introducing the sound horizon r_d as a free parameter we find for the full-data set (BAO+Pantheon-QSR-GRB+CC) $H_0 = 69.21 \pm 1.22$ Km s^{-1} Mpc^{-1} and $r_d = 133.46 \pm 2.90$ Mpc in ΛCDM model, $H_0 = 71.39 \pm 1.11$ Km s^{-1} Mpc^{-1} and $r_d = 129.57 \pm 2.64$ Mpc in wCDM model, and $H_0 = 71.43 \pm 1.01$ Km s^{-1} Mpc^{-1} and $r_d = 129.33 \pm 2.71$ Mpc in w_0w_aCDM model. Additionally, to test the statistical performance of both wCDM and w_0w_aCDM models to the standard ΛCDM model, we use the well-known information criteria [64–66] called the Akaike information criteria, namely AIC, which defined as [67]

$$\mathrm{AIC} = \chi^2_{min} + 2k, \tag{12}$$

and BIC which defined as [68]

$$\mathrm{BIC} = \chi^2_{min} + k \ln N, \tag{13}$$

where k is the number of free parameters our our model and N is the overall number of data points (in this study $N = 273$). Thus we can calculate the AIC and BIC for the standard ΛCDM, wCDM, and w_0w_aCDM models. We find for ΛCDM, wCDM, and w_0w_aCDM, respectively, AIC = [264.5, 266.8, 268.8]. On the other hand, we find, respectively, BIC =[266.7, 269.4, 271.8]. The difference between standard ΛCDM and wCDM, w_0w_aCDM in terms of AIC and BIC units are $\Delta\mathrm{AIC} = \mathrm{AIC} - \mathrm{AIC}_\Lambda$=[2.3, 4.3] and $\Delta\mathrm{BIC} = \mathrm{BIC} - \mathrm{BIC}_\Lambda$=[2.7, 5.1], respectively. These results imply that wCDM and w_0w_aCDM models have strong support in favor of them and weak evidence against them.

6. Conclusions

The standard model of cosmology faces several issues with observational experiments, specifically the 5σ difference between early [1] and late measurements of the Hubble constant [3–7].These observational discrepancies, motivate us to test the standard model and its extensions with the recent measurements of the local expansion, . We have presented 17 uncorrelated final BAO measurements from different mission surveys listed in Table 1 in order to minimize the errors due to possible correlations between different measurements. Comparing our results with the DES collaboration [50] and eBOSS collaboration [69] final results we observe that our results are consistent. Although the estimated value of the sound horizon is lower than CMB results [1], it is still in agreement with other studies [70].

Funding: This research received no external funding

Institutional Review Board Statement: Not applicable

Informed Consent Statement: Not applicable

Data Availability Statement: The data underlying this article will be shared on reasonable request to the corresponding author

Acknowledgments: We would like to thank to CONAHCYT for sponsoring this project.

Conflicts of Interest: The authors declare no conflict of interest. The funders had no role in the design of the study; in the collection, analyses, or interpretation of data; in the writing of the manuscript; or in the decision to publish the results.

References

1. Planck Collaboration. Planck 2018 results - VI. Cosmological parameters. *A&A* **2020**, *A6*, 641.
2. C. L. Bennett et al. Nine-year Wilkinson microwave anisotropy probe (WMAP) observations: final maps and results. *ApJS* **2013**, *208*, 20.
3. Adam G. Riess et al. Observational Evidence from Supernovae for an Accelerating Universe and a Cosmological Constant. *ApJ* **1998** , *116*, 1009.
4. Adam G. Riess et al. A 3% solution: determination od the Hubble constant with the Hubble space telescope and wide field camera 3. *ApJ* **2011** , *730*, 119.
5. Adam G. Riess et al. A 2.4% determination of the local value of the Hubble constant. *ApJ* **2016** , *826* , 56.
6. Adam G. Riess et al. Large Magellanic Cloud Cepheid Standards Provide a 1% Foundation for the Determination of the Hubble Constant and Stronger Evidence for Physics beyond ΛCDM. *ApJ* **2019**, *876*, 55.
7. Adam G. Riess et al. A Comprehensive Measurement of the Local Value of the Hubble Constant with 1 km/s/Mpc Uncertainty from the Hubble Space Telescope and the SH0ES Team. *ApJL* **2022**, *934*, L7.
8. Huang, QG.; Wang, K. How the dark energy can reconcile Planck with local determination of the Hubble constant. *Eur. Phys. J.* **2016**, *C 76*, 506.
9. E. Di Valentino; A. Melchiorri; J. Silk. Reconciling Planck with the local value of H0 in extended parameter space. *Physics Letters B* **2016**, *761*, 242-246.
10. Xu, L.; Huang, QG. Detecting the neutrinos mass hierarchy from cosmological data. *Sci. China Phys. Mech. Astron.* **2018**, *61*, 039521.
11. W. Yang; S. Pan; E. Di Valentino; E. N. Saridakis; S. Chakraborty. Observational constraints on one-parameter dynamical dark-energy parametrizations and the H_0 tension. *Phys. Rev. D* **2019**, *99*, 043543.
12. V. Poulin; Tristan L. Smith; T. Karwal; M. Kamionkowsk. Early Dark Energy can Resolve the Hubble Tension. *Phys. Rev. Lett.* **2019**, *122*, 221301.
13. Sunny Vagnozzi. New physics in light of the H_0 tension: An alternative view. *Phys. Rev. D* **2020**, *102*, 023518.
14. Liu, M.; Huang, Z.; Luo, X. et al. Can non-standard recombination resolve the Hubble tension?. *Sci. China Phys. Mech. Astron.* **2020**, *63*, 290405.
15. Ding, Q.; Nakama, T.; and Wang, Y. A gigaparsec-scale local void and the Hubble tension.*Sci. China Phys. Mech. Astron.* **2020**, *63*, 290403.
16. Joseph Ryan; Yun Chen; Bharat Ratra. Baryon acoustic oscillation, Hubble parameter, and angular size measurement constraints on the Hubble constant, dark energy dynamics, and spatial curvature. *MNRAS* **2019**, *488*, 3844–3856.
17. Zhao, GB.; Raveri, M.; Pogosian, L. et al. Dynamical dark energy in light of the latest observations. *Nat Astron* **2017**, *1*, 627–632.
18. Xiaolei Li; Arman Shafieloo. A Simple Phenomenological Emergent Dark Energy Model can Resolve the Hubble Tension. *ApJL* **2019**,*883*, L3.
19. Eleonora Di Valentino. Investigating Cosmic Discordance. *ApJL* **2021**, *908*, L9.
20. Haitao M.; Zhiqi H. The H_0 Tension in Non-flat QCDM Cosmology. *ApJ* **2018**, *868*, 20.
21. M. Millon et al. An exploration of systematic uncertainties in the inference of H_0 from time-delay cosmography. *A& A* **2020**, *639*, A101.
22. Kenneth C. Wong et al. H0LiCOW – XIII. A 2.4 per cent measurement of H_0 from lensed quasars: 5.3σ tension between early- and late-Universe probes. *MNRAS* **2019**, *498*, 1420–1439.
23. Mooley, K.P.; Deller, A.T.; Gottlieb, O. et al. Superluminal motion of a relativistic jet in the neutron-star merger GW170817. *Nature* **2018**, *561*, 355–359.
24. The LIGO Scientific Collaboration and The Virgo Collaboration.; The 1M2H Collaboration.; The Dark Energy Camera GW-EM Collaboration; the DES Collaboration et al. A gravitational-wave standard siren measurement of the Hubble constant. *Nature* **2017**, *551*, 85–88.
25. Hotokezaka, K.; Nakar, E.; Gottlieb, O. et al. A Hubble constant measurement from superluminal motion of the jet in GW170817. *Nat Astron* **2019**, *3*, 940–944.
26. Qin Wu et al. An 8 per cent determination of the Hubble constant from localized fast radio bursts. *MNRAS:Letters* **2022**, *515*, L1–L5.
27. C. W. James et al. A measurement of Hubble's Constant using Fast Radio Bursts. *MNRAS* **2022**, *516*, 4862–4881.

28. D. W. Pesce et al. The Megamaser Cosmology Project. XIII. Combined Hubble Constant Constraints *ApJL* **2020**, *891*, L1.
29. J. Reid et al. An Improved Distance to NGC 4258 and Its Implications for the Hubble Constant. *ApJL* **2019**, *886*, L27.
30. C. Y. Kuo et al. The Megamaser Cosmology Project. VI. Observations of NGC 6323. *ApJ* **2015**, *800*, 26.
31. Wendy L. Freedman et al. The Carnegie-Chicago Hubble Program. VIII. An Independent Determination of the Hubble Constant Based on the Tip of the Red Giant Branch. *ApJ* **2019** , *882*, 34.
32. Wendy L. Freedman et al. Calibration of the Tip of the Red Giant Branch. *ApJ* **2020**, *891*, 57.
33. Wendy L. Freedman. Measurements of the Hubble Constant: Tensions in Perspective. *ApJ* **2021**, *919*, 16.
34. G. E. Addison et al. Elucidating ΛCDM: Impact of Baryon Acoustic Oscillation Measurements on the Hubble Constant Discrepancy. *ApJ* **2021**, *853*, 119.
35. Moresco, M.; Amati, L.; Amendola, L. et al. Unveiling the Universe with emerging cosmological probes. *Living Rev Relativ* **2022**, *25*, 6.
36. S. H. Suyu et al. H0LiCOW – I. H0 Lenses in COSMOGRAIL's Wellspring: program overview. *MNRAS* **2017** , *468*, 2590–2604.
37. Kenneth C. Wong et al. H0LiCOW – XIII. A 2.4 per cent measurement of H0 from lensed quasars: 5.3σ tension between early- and late-Universe probes. *MNRAS* **2020** , *498*, 1420–1439.
38. The LIGO Scientific Collaboration and The Virgo Collaboration.; The 1M2H Collaboration.; The Dark Energy Camera GW-EM Collaboration; the DES Collaboration et al. A gravitational-wave standard siren measurement of the Hubble constant. *Nature* **2017**, *551*, 85–88.
39. Zhang, X.; Huang, Q.G.; Measuring H_0 from low-z datasets. *Sci. China Phys. Mech. Astron.* **2020**, *63*, 290402.
40. Florian Beutler et al. The 6dF Galaxy Survey: baryon acoustic oscillations and the local Hubble constant. *MNRAS* **2011**, *416*, 3017–3032.
41. Eyal A. Kazin et al. The WiggleZ Dark Energy Survey: improved distance measurements to z = 1 with reconstruction of the baryonic acoustic feature. *MNRAS* **2014**, *441*, 3524–3542.
42. Ashley J. Ross et al. The clustering of the SDSS DR7 main Galaxy sample – I. A 4 per cent distance measure at z = 0.15. *MNRAS* **2015**, *449*, 835–847.
43. Shadab Alam et al. The clustering of galaxies in the completed SDSS-III Baryon Oscillation Spectroscopic Survey: cosmological analysis of the DR12 galaxy sample. *MNRAS* **2017**, *470*, 2617–2652.
44. Srivatsan Sridhar et al. Clustering of LRGs in the DECaLS DR8 Footprint: Distance Constraints from Baryon Acoustic Oscillations Using Photometric Redshifts. *ApJ* **2020**, *904*, 69.
45. Héctor Gil-Marín et al. The Completed SDSS-IV extended Baryon Oscillation Spectroscopic Survey: measurement of the BAO and growth rate of structure of the luminous red galaxy sample from the anisotropic power spectrum between redshifts 0.6 and 1.0. *MNRAS* **2020**, *498*, 2492–2531.
46. Anand Raichoor et al. The completed SDSS-IV extended Baryon Oscillation Spectroscopic Survey: large-scale structure catalogues and measurement of the isotropic BAO between redshift 0.6 and 1.1 for the Emission Line Galaxy Sample. *MNRAS* **2021**, *500*, 3254–3274.
47. Jiamin Hou et al. The completed SDSS-IV extended Baryon Oscillation Spectroscopic Survey: BAO and RSD measurements from anisotropic clustering analysis of the quasar sample in configuration space between redshift 0.8 and 2.2. *MNRAS* **2021**, *500*, 1201–1221.
48. Hélion du Mas des Bourboux et al. he Completed SDSS-IV Extended Baryon Oscillation Spectroscopic Survey: Baryon Acoustic Oscillations with Lyα Forests. *ApJ* **2020**, *901*, 153.
49. E. de Carvalho; A. Bernui; F. Avila; C. P. Novaes; J. P. Nogueira-Cavalcante. BAO angular scale at zeff = 0.11 with the SDSS blue galaxies. *A& A* **2021**, *649*, A20.
50. T. M. C. Abbott et al. (DES Collaboration). Dark Energy Survey Year 3 results: A 2.7% measurement of baryon acoustic oscillation distance scale at redshift 0.835. *Phys. Rev. D* **2022**, *105*, 043512.
51. Lavrentios Kazantzidis; Leandros Perivolaropoulos. Evolution of the fσ8 tension with the Planck15/ΛCDM determination and implications for modified gravity theories *Phys. Rev. D* **2018**, *97*, 103503.
52. Eric V. Linder. Probing gravitation, dark energy, and acceleration *Phys. Rev. D* **2004**, *70*, 023511.
53. M. Chevallier; D. Polarski. Accelerating universes with scaling dark matter. *International Journal of Modern Physics D* **2001**, *10:02*, 213-223.
54. Eric V. Linder. Exploring the Expansion History of the Universe. *Phys. Rev. Lett.* **2003**, *90*, 091301.
55. W. J. Handley et al. POLYCHORD: nested sampling for cosmology. *MNRAS:Letters* **2015**, *450*, L61–L65.

56. D. M. Scolnic et al. The Complete Light-curve Sample of Spectroscopically Confirmed SNe Ia from Pan-STARRS1 and Cosmological Constraints from the Combined Pantheon Sample. *ApJ* **2018**, *859*, 101.
57. Michele Moresco. Raising the bar: new constraints on the Hubble parameter with cosmic chronometers at z≈2. *MNRAS:Letters* **2015**, *450*, L16–L20.
58. G. Risaliti; E. Lusso. A Hubble diagram for quasars. *ApJ* **2015**, *815*, 33.
59. Marek Demianski; Ester Piedipalumbo; Disha Sawant; Lorenzo Amati. Cosmology with gamma-ray bursts - I. The Hubble diagram through the calibrated Ep,i–Eiso correlation. *A& A* **2017**, *598*, A112.
60. Licia Verde et al. The length of the low-redshift standard ruler. *MNRAS* **2017**, *467*, 731–736.
61. José Luis Bernal et al. The trouble with H_0. *JCAP* **2016**, *10*, 019.
62. Nunes, R.C.; Bernui, A. BAO signatures in the 2-point angular correlations and the Hubble tension. *Eur. Phys. J. C* **2020**, *80*, 1025.
63. Lemos, T. et al. Low-redshift estimates of the absolute scale of baryon acoustic oscillations. *Eur. Phys. J. C* **2023**, *83*, 495.
64. Andrew R. Liddle. Information criteria for astrophysical model selection. *MNRAS:Letters* **2007**, *377*, L74–L78.
65. Fotios K. Anagnostopoulos; Spyros Basilakos; Emmanuel N. Saridakis. Bayesian analysis of f(T) gravity using $f\sigma_8$ data. *Phys. Rev. D* **2019**, *100*, 083517.
66. Burnham, K. P.; Anderson, D. R. Multimodel Inference: Understanding AIC and BIC in Model Selection. *Sociological Methods and Research* **2004**, *33(2)*, 261–304.
67. H. Akaike. A new look at the statistical model identification. *IEEE Transactions on Automatic Control* **1974**, *19(6)*, 716-723.
68. Gideon Schwarz. Estimating the Dimension of a Model. *Ann. Statist.* **1978**, *6(2)*, 461-464.
69. Shadab Alam et al. Completed SDSS-IV extended Baryon Oscillation Spectroscopic Survey: Cosmological implications from two decades of spectroscopic surveys at the Apache Point Observatory. *Phys. Rev. D* **2021**, *103*, 083533.
70. Radosław Wojtak ; Adriano Agnello. The Hubble–Lemaître constant and sound horizon from low-redshift probes. *MNRAS* **2019**, *486*, 5046–5051.